JACS
JOURNAL OF THE AMERICAN CHEMICAL SOCIETY

Communication

pubs.acs.org/JACS

Identification of a Catalytic Iron-Hydride at the H-Cluster of [FeFe]-Hydrogenase

David W. Mulder,[†,§] Yisong Guo,*[,‡,§] Michael W. Ratzloff,[†] and Paul W. King*[,†]

[†]Biosciences Center, National Renewable Energy Laboratory, Golden, Colorado 80401, United States
[‡]Department of Chemistry, Carnegie Mellon University, Pittsburgh, Pennsylvania 15213, United States

Supporting Information

ABSTRACT: Hydrogenases couple electrochemical potential to the reversible chemical transformation of H_2 and protons, yet the reaction mechanism and composition of intermediates are not fully understood. In this Communication we describe the biophysical properties of a hydride-bound state (H_{hyd}) of the [FeFe]-hydrogenase from *Chlamydomonas reinhardtii*. The catalytic H-cluster of [FeFe]-hydrogenase consists of a [4Fe-4S] subcluster ($[4Fe\text{-}4S]_H$) linked by a cysteine thiol to an azadithiolate-bridged 2Fe subcluster ($[2Fe]_H$) with CO and CN^- ligands. Mössbauer analysis and density functional theory (DFT) calculations show that H_{hyd} consists of a reduced $[4Fe\text{-}4S]_H^+$ coupled to a diferrous $[2Fe]_H$ with a terminally bound Fe-hydride. The existence of the Fe-hydride in H_{hyd} was demonstrated by an unusually low Mössbauer isomer shift of the distal Fe of the $[2Fe]_H$ subcluster. A DFT model of H_{hyd} shows that the Fe-hydride is part of a H-bonding network with the nearby bridging azadithiolate to facilitate fast proton exchange and catalytic turnover.

The catalytic domain of [FeFe]-hydrogenase ([FeFe]-H_2ases) harbors a unique iron−sulfur cofactor, or H-cluster, comprised of a [4Fe-4S] subcluster ($[4Fe\text{-}4S]_H$) linked by a Cys residue thiol to an organometallic 2Fe subcluster ($[2Fe]_H$) containing CO, CN^-, and azadithiolate (adt) ligands (Figure 1).[1−3] Proton-exchangeable groups within H-bonding distance to the H-cluster include the bridgehead amine of adt, and conserved Lys and Cys residues.[4] Electrons are exchanged with physiological donors/acceptors through the $[4Fe\text{-}4S]_H$.[5−7] Redox states of the H-cluster have been described that include the oxidized (H_{ox}), one-electron-reduced (H_{red} and H_{red}'), and two-electron-reduced (H_{sred}) states.[5,8−10] However, a complete description of an Fe-hydride species of the H-cluster predicted by heterolytic H_2 activation mechanism has not yet been described.

Density functional theory (DFT) studies show that H_2 binding and activation are favorable at the exchangeable site located at the distal Fe atom of $[2Fe]_H$ (Fe_d) in the Fe(II) oxidation state.[11] However, the involvement of a bridging versus a terminal hydride (H^-) intermediate in the catalytic mechanism remains unresolved.[12] The steric constraints on H-cluster dynamics by the surrounding protein environment and regiochemistry of the terminal site favor a catalytic mechanism involving a terminal hydride.[13] This model is reflected in mechanisms of H-cluster mimics that exhibit faster and more reversible H_2 activation when involving terminal hydride intermediates.[14,15]

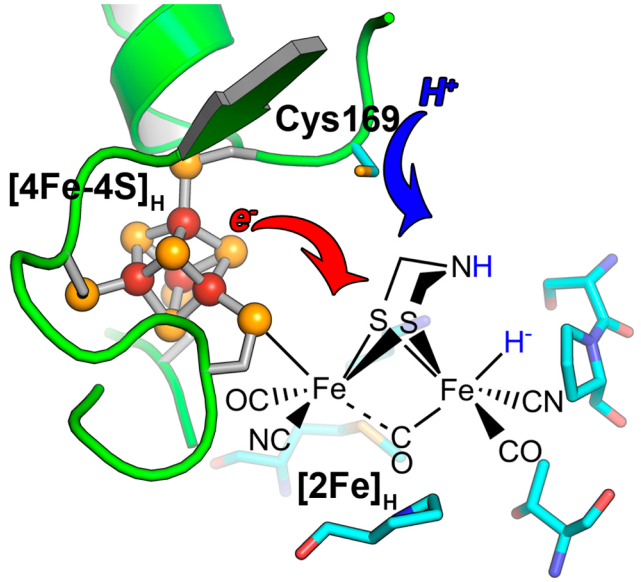

Figure 1. Active-site H-cluster of [FeFe]-H_2ase *Cr*HydA1. The result of proton (blue arrow) and electron (red arrow) transfer is depicted to show formation of a terminal Fe-hydride. The oxidation state of the H-cluster and the protonation structure are addressed herein. The surrounding protein framework (from PDB 3LX4) of $[4Fe\text{-}4S]_H$ is green, and that of $[2Fe]_H$ is cyan.

The [FeFe]-H_2ase from *Chlamydomonas reinhardtii* (*Cr*HydA1) possesses a catalytic domain and H-cluster, and is a low-complexity model to investigate the H_2 activation mechanism. Our previous electron paramagnetic resonance (EPR) and Fourier-transform infrared (FTIR) studies of reduced native and Cys-to-Ser variant (C169S) forms of *Cr*HydA1 identified an H-cluster state with properties suggestive of a hydride bound at $[2Fe]_H$ (H_{hyd}, Figure 1).[16] The exchange of Cys-to-Ser in C169S is proposed to alter the proton-transfer kinetics to result in the enrichment of H_{hyd}. The presence of an Fe-hydride species is indicated from hydrogen−deuterium (H/D) isotope FTIR spectra of both native *Cr*HydA1 and the C169S variant, which displayed an H/D isotope shift of the $[2Fe]_H$ bridging CO mode. The H/D isotope effect was best simulated by DFT

Received: November 7, 2016
Published: December 14, 2016

DOI: 10.1021/jacs.6b11409
J. Am. Chem. Soc. 2017, 139, 83−86

as a H-cluster model in an $[4Fe\text{-}4S]_H^+$–$Fe^{II}Fe^{II}$–H^- configuration.[16]

Herein, using Mössbauer spectroscopy and DFT modeling, we substantiate the formation of an Fe-hydride moiety in H_{hyd} and further reveal the electronic and geometric structures of the Fe-hydride bond. The Mössbauer isomer shift values of $[2Fe]_H$ in H_{hyd} are consistent with a terminal hydride on Fe_d of $[2Fe]_H$ of a H-cluster in an $[4Fe\text{-}4S]_H^+$–$Fe^{II}Fe^{II}$–H^- configuration. An EPR-monitored redox titration of C169S shows that the H_{red}→H_{hyd} redox transition and hydride formation occurs near the H^+/H_2 redox potential, whereas the H_{ox}→H_{red} transition is shifted to a more positive value compared to the value determined for native *Cr*HydA1.[17] This, combined with slow proton transfer for protonation/deprotonation of H_{hyd}, explains the enrichment of H_{hyd} in C169S and provides further insight into the proton-transfer steps in the mechanism of [FeFe]-H_2ase.

Isolation of H_{hyd} in sodium dithionite (NaDT)-reduced C169S was first confirmed by EPR and IR measurements (Figures S1 and S2). The 4.2 K low-field Mössbauer spectra of H_{hyd}-enriched preparations of C169S show two quadrupole doublets located in the velocity range of −1.0 to 1.0 mm/s and magnetic splitting features extending from −3.0 to 4.0 mm/s (Figure 2A and Figures S6 and S8). The spectrum collected under zero applied field clearly demonstrated that the two doublets have ∼1:1 ratio of the absorption area (Figure S4). The spectral simulations revealed that each quadrupole doublet represents ∼13% of the total iron in the sample, but with very different isomer shifts (doublet I: δ_I = 0.23 mm/s, $|\Delta E_{QI}|$ = 1.06; and doublet II: δ_{II} = 0.03 mm/s, $|\Delta E_{QII}|$ = 0.68). These isomer shift values fall into the range of those from low oxidation state iron (Fe^I or Fe^{II}) carbonyl complexes;[18−21] thus, they can be assigned to originate from the $[2Fe]_H$ subcluster. The low isomer shift value (0.03 mm/s) for doublet II has not been previously observed in [FeFe]-H_2ases, indicating unique coordination/oxidation status of this iron site.

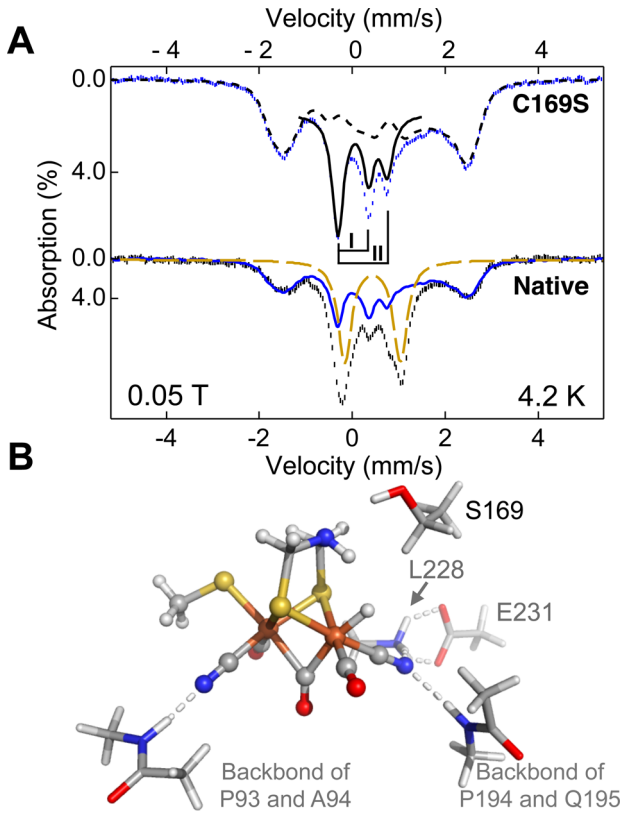

Figure 2. (A) Mössbauer spectra of NaDT-reduced ^{57}Fe-labeled C169S (top, blue vertical bars) and native *Cr*HydA1 (bottom, black vertical bars), and spectral simulations of $[4Fe\text{-}4S]^+$ (black dotted line), $[2Fe]_H$ (black solid line), and $[4Fe\text{-}4S]^{2+}$ (gold dashed line). Refer to Tables S1 and S2 for detailed spectral simulation parameters. (B) DFT-optimized structure of the $[2Fe]_H$ subcluster containing a terminal Fe-hydride that best reproduces the experimental Mössbauer parameters of H_{hyd}. Amino acid numbering refers to the *Cr*HydA1 protein sequence. Color code: iron, brown; sulfur, yellow; oxygen, red; nitrogen, blue; carbon, grey; hydrogen, white.

Variable-field and variable-temperature Mössbauer measurements were also performed (Figures S5−S7, Tables S1 and S2). The subsequent spectral analysis revealed that doublets I and II belong to diamagnetic species (S = 0), and the magnetic splitting features can be assigned to a single type of S = 1/2 $[4Fe\text{−}4S]^+$ cluster that occupies ∼58% of the total iron in the sample (see Supporting Information for detailed analysis). It is important to notice that the ratio of the absorption areas from $[4Fe\text{-}4S]_H^+$ relative to $[2Fe]_H$ (sum of the absorption areas from doublets I and II) is ∼2:1 (58%:26%), indicating that they belong to the same H-cluster state. Collectively, this H-cluster state represents ∼80% of the total iron in the sample. Together with the EPR spin quantification results, it is revealed that NaDT-reduced C169S *Cr*HydA1 contains predominantly a single H-cluster state assigned to H_{hyd}.

We have shown by EPR and IR spectroscopy that H_{hyd} can also be observed in reduced native *Cr*HydA1 (Figures S1 and S2),[16] albeit at lower levels due to the faster rates of proton exchange and turnover.[6,16] Based on the Mössbauer parameters of H_{hyd} from C169S, the fraction of H_{hyd} in NaDT-reduced native *Cr*HydA1 was ∼45−50% of the total iron in the sample (Figure 2A). The majority of the remaining iron can be assigned to the H_{red} state that is identified by an EPR-silent S = 0 $[4Fe\text{-}4S]^{2+}$ subcluster (δ = 0.45 mm/s, ΔE_Q = 1.10 mm/s), representing ∼30% of the total iron (gold dashed line in Figure 2A). The H_{red} state consists of a diamagnetic H-cluster having a $[4Fe\text{-}4S]_H^{2+}$ paired with an Fe^IFe^I $[2Fe]_H$.[22,23] Due to the lack of spectral resolution in the center part of the spectra, the spectral features of the H_{red} $[2Fe]_H$ subcluster cannot be uniquely determined, and thus detailed simulations were not attempted. IR spectra further support the presence of H_{red} with ν(CO) peaks characteristic of this state (Figure S2).[16] Altogether, H_{hyd} was observed in the Mössbauer spectra of both native and C169S *Cr*HydA1 under catalytic conditions.

DFT calculations were carried out to provide further structural insights into the $[2Fe]_H$ subcluster in the spectroscopically characterized H_{hyd} species (see Supporting Information for details, including Figures S9−S16 and Tables S3−S6). While there are several extensive DFT studies to identify the IR features associated with different H-cluster states,[24−27] there are none for predicting Mössbauer parameters of H-clusters in enzymes. Here, DFT calculations were carried out using different structural and oxidation-state models of the $[2Fe]_H$ subcluster of the H-cluster. The validity of the DFT models was verified by comparing the calculated Mössbauer parameters, such as isomer shifts (δ) and quadrupole splittings (ΔE_Q), as well as ν(CO) frequencies, with the experimental values.

A structural model of the $[2Fe]_H$ subcluster in H_{hyd} that best fits to the collective spectral properties is a diamagnetic $[2Fe]_H$ in an $Fe^{II}Fe^{II}$ oxidation state with a terminal Fe-hydride on the

DOI: 10.1021/jacs.6b11409
J. Am. Chem. Soc. 2017, 139, 83−86

Fe_d site and an unprotonated amine of the adt group (Figure 2B and Model 1 in Figure S14). An Fe(II)-H^- species best accounts for the low Mössbauer isomer shift value (δ = 0.03 mm/s) of doublet II. The large isomer shift difference (~0.2 mm/s) between the two iron sites of the $[2Fe]_H$ in H_{hyd} at the same Fe(II) oxidation state is intriguing. It is reproduced by the Fe_d(II)-H^- model[28] and can be explained as the consequence of the strong Fe−H^- interaction at the Fe_d site, which is reflected by a short Fe−H^- bond (1.52 Å) predicted by DFT (Figure S14). The strong Fe−H^- interaction enables strong charge donation of H^- to the valence 4s orbital of the Fe_d site, which increases the s electron density of iron and lowers its isomer shift.[29] These findings agree with a recent Mössbauer study on a low-spin iron (Fe^{II}) phosphine model compound. With and without the presence of an Fe-bound hydride, the isomer shift differed by ~0.2 mm/s, with the hydride-bound form having the lower value.[30] Likewise, it has been shown for a functional [NiFe]-H_2ase model compound that the presence of a hydride at the Fe site accounts for its lower isomer shift value.[31]

To determine the catalytic relevance of H_{hyd} for H_2 activation, an EPR-monitored steady-state redox titration was carried out on the C169S variant. The slower turnover rate (~100×)[16] compared to that of the native *Cr*HydA1 made it possible to titrate the enzyme over a wide potential range with only small amounts of drift at low potentials due to proton reduction/H_2 formation (Figure 3). Starting from the reduced sample showing the predominant H_{hyd} species with g_{max} = 2.07, the overall EPR signal attenuated as the potential became more positive, which is consistent with the formation of H_{red}, an EPR-silent species.[17,32] By further increasing the potential, the appearance of the characteristic rhombic g_{max} = 2.1 (g = 2.1, 2.04, 1.99), reflective of H_{ox}, was observed. Upon reversing the titration back to the reducing direction using NaDT, the H_{ox} state converted to H_{red}, as observed by the attenuation of the overall EPR signal, followed by re-formation of H_{hyd}, evidenced by the appearance of the g_{max} = 2.07 signal. Overall, the titration demonstrates the reversible formation of H_{hyd}, H_{red}, and H_{ox} redox intermediates. Midpoint potentials at pH 8 ($E_{m,8}$) for the H_{hyd} ($E_{m,8}$ = −431 mV) and H_{ox} ($E_{m,8}$ = −283 mV) species were determined by fitting signal intensities to the n = 1 Nernst equation (Figure S3). The E_m for H_{red} ($E_{m,8}$ = −357 mV) was estimated from the plot of the spin quantification of the overall signal (Figure S3). The fact that reversible formation of H_{hyd} occurs near the H^+/H_2 redox potential (−448 mV at pH 8) confirms its role as the key H_2 activation step in the catalytic cycle.

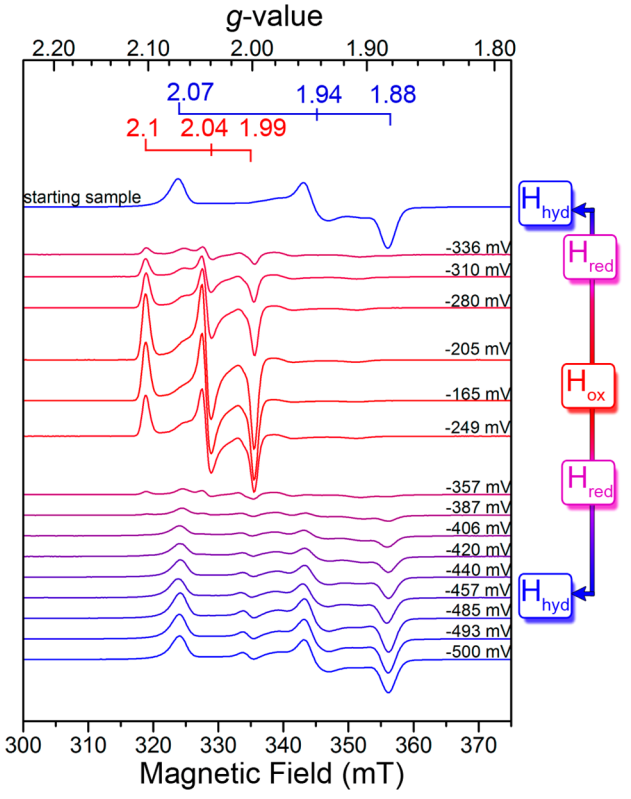

Figure 3. EPR-monitored redox titration of the H-cluster from the *Cr*HydA1 C169S variant. EPR spectra (9.38 GHz, 1 mW microwave power, T = 17 K) were collected from *Cr*HydA1 C169S samples (102 μM, 299 K, pH 8) poised at the respective potentials (versus SHE) by titration in a buffered solution (pH 8) containing redox mediators using either sodium dithionite for reduction or indigo disulfonate for oxidation.

Compared to the native enzyme ($E_{m,8}$ = −400 mV),[17] the E_m for the H_{ox}-to-H_{red} transition in the C169S variant is shifted to a more positive value ($E_{m,8}$ = −283 mV). This reveals that the Cys-to-Ser change, in addition to altering the proton-transfer kinetics, significantly alters the thermodynamic properties of the H-cluster. The changes in these properties account for enrichment of H_{hyd} over H_{red} in C169S under the reducing conditions used here. Altogether, H_{hyd} can be rationally assigned in the catalytic model, where protonation of H_{hyd} leads to H_2 formation and release to re-form H_{ox} (Figure 4).

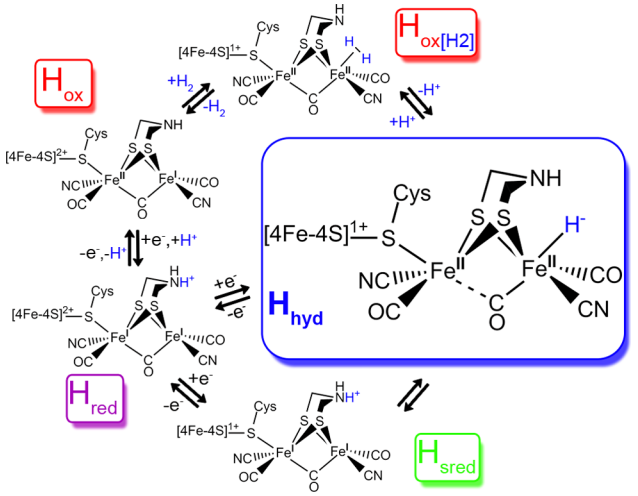

Figure 4. Catalytic model showing the role of H_{hyd} in reversible H_2 activation at the H-cluster. The protons (H^+) shown above the reaction arrows originate from solvent via the proton-transfer pathway in *Cr*HydA1 that leads to the Cys169 residue. The terminal hydride (H^-) in H_{hyd} is modeled to result from intramolecular proton transfer from the bridging amine ($-NH_2$) to Fe_d of $[2Fe]_H$.

In summary, the altered proton-transfer kinetics and thermodynamics of the C169S *Cr*HydA1 were used to determine the properties of an Fe-hydride in the H_{hyd} state of [FeFe]-H_2ase. There is precedent for a similar Fe-hydride-dependent mechanism in synthetic mono-Fe complexes, where heterolytic bond cleavage of H_2 on an Fe(II) center forms a terminal Fe(II)−H^-, has been observed by neutron diffraction crystallography.[33] The altered redox potentials of the H_{ox}→H_{red}

DOI: 10.1021/jacs.6b11409
J. Am. Chem. Soc. 2017, 139, 83−86

catalytic transition caused by the Cys-to-Ser change signify an underlying role of the secondary coordination sphere in tuning the reactivity and redox couples of the H-cluster. They also illustrate how the H-cluster is finely tuned for proton-coupled electron transfer through a combination of electronic structures of the H-cluster and the surrounding protein environment.

■ ASSOCIATED CONTENT

Supporting Information

The Supporting Information is available free of charge on the ACS Publications website at DOI: 10.1021/jacs.6b11409.

Materials and methods; additional EPR, IR, Mössbauer, and DFT figures and analysis including Figures S1−S16 and Tables S1−S6 (PDF)

■ AUTHOR INFORMATION

Corresponding Authors

*ysguo@andrew.cmu.edu
*paul.king@nrel.gov

ORCID

Yisong Guo: 0000-0002-4132-3565
Paul W. King: 0000-0001-5039-654X

Author Contributions

§D.W.M. and Y.G. contributed equally.

Notes

The authors declare no competing financial interest.

■ ACKNOWLEDGMENTS

Native and C169S variant *Cr*HydA1 sample preparation, FTIR spectroscopy, and EPR redox titration experiments were performed at NREL under support from the U.S. Department of Energy, Office of Basic Energy Sciences, Division of Chemical Sciences, Geosciences, and Biosciences, and the U.S. Department of Energy under Contract No. DE-AC36-08-GO28308. Y.G. acknowledges financial support from Carnegie Mellon University and thanks Mr. Ruixi Fan for assistance with Mössbauer measurements and DFT calculations.

■ REFERENCES

(1) Peters, J. W.; Lanzilotta, W. N.; Lemon, B. J.; Seefeldt, L. C. *Science* **1998**, *282*, 1853.
(2) Nicolet, Y.; Piras, C.; Legrand, P.; Hatchikian, C. E.; Fontecilla-Camps, J. C. *Structure* **1999**, *7*, 13.
(3) Silakov, A.; Wenk, B.; Reijerse, E.; Lubitz, W. *Phys. Chem. Chem. Phys.* **2009**, *11*, 6592.
(4) Winkler, M.; Esselborn, J.; Happe, T. *Biochim. Biophys. Acta, Bioenerg.* **2013**, *1827*, 974.
(5) Adamska, A.; Silakov, A.; Lambertz, C.; Rudiger, O.; Happe, T.; Reijerse, E.; Lubitz, W. *Angew. Chem., Int. Ed.* **2012**, *51*, 11458.
(6) Mulder, D. W.; Ratzloff, M. W.; Shepard, E. M.; Byer, A. S.; Noone, S. M.; Peters, J. W.; Broderick, J. B.; King, P. W. *J. Am. Chem. Soc.* **2013**, *135*, 6921.
(7) Lambertz, C.; Chernev, P.; Klingan, K.; Leidel, N.; Sigfridsson, K. G. V.; Happe, T.; Haumann, M. *Chem. Sci.* **2014**, *5*, 1187.
(8) Chernev, P.; Lambertz, C.; Brünje, A.; Leidel, N.; Sigfridsson, K. G. V.; Kositzki, R.; Hsieh, C.-H.; Yao, S.; Schiwon, R.; Driess, M.; Limberg, C.; Happe, T.; Haumann, M. *Inorg. Chem.* **2014**, *53*, 12164.
(9) Adamska-Venkatesh, A.; Krawietz, D.; Siebel, J.; Weber, K.; Happe, T.; Reijerse, E.; Lubitz, W. *J. Am. Chem. Soc.* **2014**, *136*, 11339.
(10) Katz, S.; Noth, J.; Horch, M.; Shafaat, H.; Happe, T.; Hildebrandt, P.; Zebger, I. *Chem. Sci.* **2016**, *7*, 6746.
(11) Fan, H. J.; Hall, M. B. *J. Am. Chem. Soc.* **2001**, *123*, 3828.
(12) Leidel, N.; Hsieh, C.-H.; Chernev, P.; Sigfridsson, K. G.; Darensbourg, M. Y.; Haumann, M. *Dalton Trans.* **2013**, *42*, 7539.
(13) Finkelmann, A. R.; Stiebritz, M. T.; Reiher, M. *Chem. Sci.* **2014**, *5*, 215.
(14) Camara, J. M.; Rauchfuss, T. B. *Nat. Chem.* **2012**, *4*, 26.
(15) Schilter, D.; Camara, J. M.; Huynh, M. T.; Hammes-Schiffer, S.; Rauchfuss, T. B. *Chem. Rev.* **2016**, *116*, 8693.
(16) Mulder, D. W.; Ratzloff, M. W.; Bruschi, M.; Greco, C.; Koonce, E.; Peters, J. W.; King, P. W. *J. Am. Chem. Soc.* **2014**, *136*, 15394.
(17) Silakov, A.; Kamp, C.; Reijerse, E.; Happe, T.; Lubitz, W. *Biochemistry* **2009**, *48*, 7780.
(18) Razavet, M.; Davies, S. C.; Hughes, D. L.; Barclay, J. E.; Evans, D. J.; Fairhurst, S. A.; Liu, X.; Pickett, C. J. *Dalton Trans.* **2003**, 586.
(19) Hsieh, C.-H.; Erdem, O. z. F.; Harman, S. D.; Singleton, M. L.; Reijerse, E.; Lubitz, W.; Popescu, C. V.; Reibenspies, J. H.; Brothers, S. M.; Hall, M. B.; Darensbourg, M. Y. *J. Am. Chem. Soc.* **2012**, *134*, 13089.
(20) Silakov, A.; Olsen, M. T.; Sproules, S.; Reijerse, E. J.; Rauchfuss, T. B.; Lubitz, W. *Inorg. Chem.* **2012**, *51*, 8617.
(21) Stoian, S. A.; Hsieh, C.-H.; Singleton, M. L.; Casuras, A. F.; Darensbourg, M. Y.; McNeely, K.; Sweely, K.; Popescu, C. V. *J. Biol. Inorg. Chem.* **2013**, *18*, 609.
(22) Pereira, A. S.; Tavares, P.; Moura, I.; Moura, J. J. G.; Huynh, B. H. *J. Am. Chem. Soc.* **2001**, *123*, 2771.
(23) Popescu, C. V.; Münck, E. *J. Am. Chem. Soc.* **1999**, *121*, 7877.
(24) Cao, Z.; Hall, M. B. *J. Am. Chem. Soc.* **2001**, *123*, 3734.
(25) Liu, Z.-P.; Hu, P. *J. Am. Chem. Soc.* **2002**, *124*, 5175.
(26) Yu, L.; Greco, C.; Bruschi, M.; Ryde, U.; De Gioia, L.; Reiher, M. *Inorg. Chem.* **2011**, *50*, 3888.
(27) Tye, J. W.; Darensbourg, M. Y.; Hall, M. B. *Inorg. Chem.* **2008**, *47*, 2380.
(28) The observation of a difference in isomer shifts for the two iron sites in $[2Fe]_H$ is not conclusive evidence for the existence of a terminally bound hydride on the Fe_d site. As shown in Figure S16 and Table S6, nearly every DFT model structure has predicted differences in the isomer shifts for the two iron sites. Yet, only Model 1 shown in Figures 2B and S14 nicely reproduces both the Mössbauer parameters and the ν(CO) IR frequencies measured here.
(29) Gütlich, P.; Bill, E.; Trautwein, A. X. *Mössbauer spectroscopy and transition metal chemistry: fundamentals and applications*; Springer: Heidelberg, 2010.
(30) Weber, K.; Weyhermüller, T.; Bill, E.; Erdem, Ö. F.; Lubitz, W. *Inorg. Chem.* **2015**, *54*, 6928.
(31) Kochem, A.; Bill, E.; Neese, F.; van Gastel, M. *Chem. Commun.* **2015**, *51*, 2099.
(32) Roseboom, W.; De Lacey, A. L.; Fernandez, V. M.; Hatchikian, E. C.; Albracht, S. P. J. *JBIC, J. Biol. Inorg. Chem.* **2006**, *11*, 102.
(33) Liu, T.; Wang, X.; Hoffmann, C.; DuBois, D. L.; Bullock, R. M. *Angew. Chem., Int. Ed.* **2014**, *53*, 5300.

DOI: 10.1021/jacs.6b11409
J. Am. Chem. Soc. 2017, 139, 83−86